Slot-Die Coating of Perovskite Solar Cells: An Overview

Rahul Patidar, Daniel Burkitt, Katherine Hooper, David Richards, Trystan Watson

SPECIFIC, Baglan Bay Innovation Centre, Central Avenue, Baglan, Port Talbot, SA12 7AX.

Abstract

To make perovskite solar cells an industrially relevant technology large area deposition techniques are needed and one of the most promising is slot-die coating. This review article details the progress reported in the literature where slot-die coating has been used for the deposition of both the perovskite layer and other layers in the perovskite solar cell device stack. An overview of the methods used to adapt the coating process, materials and drying conditions in order to create high quality layers and devices is given and an outlook on future research directions in this field is made.

Keywords: Slot-die Coating, Perovskite Solar Cell, Manufacturing, Photovoltaics, Roll-to-Roll

1. Introduction

The remarkable opto-electronic properties of lead halide perovskites coupled with the advancements in thin film photovoltaic device fabrication generated from organic photovoltaic (OPV) and dye sensitised solar cell (DSSC) research has propelled perovskite solar cells (PSC) to astonishing power conversion efficiencies (PCEs) and the forefront of next generation photovoltaics research. In under a decade PCEs rose from 3.8% in 2009 to certified 24.2% as of July 2019, outperforming well established technologies like multicrystalline silicon and copper indium gallium selenide solar cells (CIGS) [1, 2, 3, 4, 5].

PSCs show great potential in becoming a disruptive technology in the photovoltaics industry, however, there are many challenges yet to overcome to bring this technology to the market. For instance, bridging the 'scaling gap' and transitioning PSCs from a lab scale to an industrial scale is a serious challenge [6]. Compatibility with flexible substrates and devices and the potential for high throughput roll-to-roll (R2R) manufacture that this offers is one of the key features that makes the case for using PSCs compelling. R2R fabrication not only offers the possibility of manufacturing at far higher speeds than those possible for conventional silicon photovoltaics but also offers the opportunity to deploy modules at unprecedented rates and in novel formats, as demonstrated for structurally similar organic photovoltaics [7, 8].

Efforts are being made to upscale the technology with a variety of techniques having been employed for the fabrication of large area PSCs, utilising both solution based and vacuum deposition methods. The most common are spin coating, blade coating [9], screen printing [10], spray coating [11, 12], slot-die coating, gravure printing [13] and vacuum deposition [14]. It could be argued that, to date, the most successful of these is blade coating where it has been used for the deposition of the perovskite layer in modules with PCEs of over 15% and an aperture area of 30cm^2 [15]. Blade coating of perovskites has only been reported for small scale bench-top sheet-to-sheet (S2S) fabrication and not for R2R processes. Only gravure [13] and slot-die coating [16, 17, 18, 19, 20, 21] have been reported for use in R2R deposition processes for the perovskite layer of the device stack, with slot-die coating resulting in devices achieving both high PCEs and line speeds on flexible glass [20] and plastic substrates [19].

Slot-die coating is well suited for the deposition of perovskite inks, as well as other layers in the device stack. As a pre-metered coating method, it is highly efficient in terms of materials usage and results in very low wastage levels of inks compared to other deposition methods such as spin coating or spray and screen printing. For a typical slot-die coating process a coating head is positioned close to and across a substrate or web, ink is then pumped into the head, using a syringe pump, with the ink forced out of a narrow slit along the length of the coating head (Figure 1).

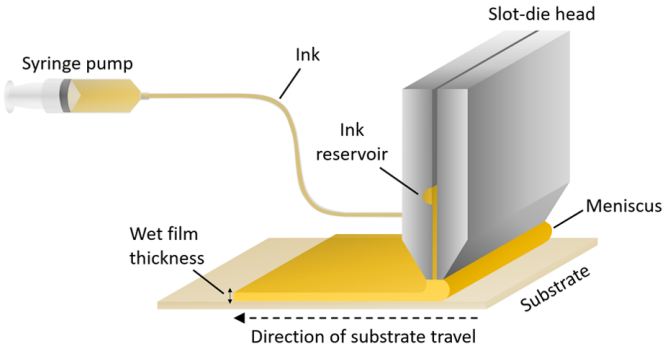

Figure 1: Schematic of a slot-die coating process, showing the delivery of ink to the head from a syringe pump and formation of an ink wet film between the coating head lips and the substrate.

The ink forms a liquid bridge between the coating head and the substrate whereby when the substrate is moved past the head, the deposition of a wet film is achieved. Over a given coating width the thickness of the dry film deposited is controlled by adjusting the flow of ink to the coating head and the

speed at which the substrate moves past the head. This directly translates to changes in the wet film thickness and subsequently after drying the dry film thickness. This allows for very fine control of the dry film thickness, to within a few nm, as well as the ability to deposit very thin dry films, of tens of nm, up to much thicker films of tens of microns simply by adjusting the ink flow rate or substrate speed.

There are a number of common failure mechanisms for slot-die coatings including (i) the 'low-flow' limit [22], where the breakup of the downstream meniscus causes discontinuity in the wet film (ii) discontinuous film defects such as rivulets, where the coating breaks into multiple smaller stripes with gaps (iii) completely discontinuous films where the coating stops and starts along the length of the substrate (iv) air-entrainment defects, associated with the breakup of the upstream meniscus leading to 'bubbles' within the wet film and areas of uncoated substrate and (v) 'flooding' or 'dripping' where the flow of ink to the head is too great compared to the coating speed and results in the gradual build-up of ink at the coating head and loss of pre-metering and the expected film thickness. One of the most important operating limits is the low-flow limit, which causes break-up of the down stream meniscus and discontinous film formation. The capillary number is given by 1 and the low-flow limit can be given in terms of a critical capillary number ($Ca_{low-flow}$) as in 2, above which, for a particular gap height and wet film thickness, the coating is unstable, the low-flow limit is generally applicable for capillary numbers less than one but deviations can occur for higher capillary numbers. Here μ is the viscosity of the ink, σ is surface tension, V is the web speed or coating speed, H is the gap between substrate and die head and t is the wet film thickness. Therefore, for the set operating parameters H and V, the ink rheology (surface tension and viscosity) must be adjusted (or vice-versa) to remain below critical capillary number ensuring defect free films with right wet film thickness. For a more complete explanation of slot-die coating and common defects the reader is directed to the review article by Harris et al. [23].

$$Ca = \frac{\mu V}{\sigma} \tag{1}$$

$$Ca_{low-flow} = \frac{\mu V}{\sigma} \leq 0.65\left(\frac{2}{\frac{H}{t}-1}\right)^{\frac{3}{2}} \tag{2}$$

Table 1 summarises the device stacks and current density - voltage (JV) scan photovoltaic performance parameters for perovskite solar cells with a slot-die coated perovskite layer reported in the literature so far.

In this review, the summary of various approaches developed to slot-die coat perovskite and other layers of the device stack will be presented. The effects of different coating procedures, additives and drying conditions will be discussed, along with discussion on the fundamental understanding of nucleation and crystallization of slot-die coated perovskite films. A comprehensive review of the development in the performance of slot-die coated perovskite solar cells will be given.

2. Perovskite Film Formation

The perovskite layer is the most important layer in the perovskite solar cell device stack, to this end it is vital to have defect free films with large grain size, crystal phase purity and good film coverage that can deliver higher photovoltaic performance and stability. The following sections will discuss the various procedures developed to improve the quality of slot-die coated perovskite layers, all of which are effectively based on controlling the crystallization dynamics of the perovskite material.

2.1. Two-Step

The two-step or sequential deposition process for the fabrication of organic-inorganic perovskite layers was first introduced by Mitzi et al. [24] and later further developed for deposition of the active layer in PSCs by Burschka et al. [25]. In this process a pre-deposited lead halide film is exposed to a cation and halide source e.g. methylammonium iodide (MAI) or caesium iodide, that then react together to form the final perovskite. Most typically this is achieved by spin coating a lead iodide (PbI_2) film that is then dried and exposed to a solution of MAI either by spin coating the solution on top of the PbI_2 film or dipping the PbI_2 film into a solution of MAI. When this is applied to slot-die coating, the principal of the process is the same, with a PbI_2 layer first slot-die coated onto the substrate and the film dried, followed by either slot-die coating of a MAI solution onto the PbI_2 layer or dip coating of the PbI_2 layer in a MAI solution.

Compared to depositing the perovskite precursors from a single ink in one coating stage, termed a 'one-step' or 'single step' process, the two-step process allows the separation of film formation into distinct parts that might be beneficial to the overall film formation. When considering the formation of the perovskite film, the nucleation and crystal growth of the perovskite from the wet film of the precursor solution is critical to achieving good dry film formation with good overall film coverage. This is particularly challenging when using many of the strongly polar aprotic solvents commonly used for perovskite precursor inks. These inks, which poorly wet on many of the common interlayers, can lead to de-wetting of the substrate as well as the growth of large crystals with large voids, that when fabricated into devices lead to shunt leakages and shorts that are detrimental to performance. This was overcome in spin coated layers by depositing the lead iodide first, separately to the other precursors, which resulted in films with high surface coverage that could then be converted to perovskite to a high degree. Later this was somewhat superseded by the development of the 'anti-solvent' or 'solvent quenching' method [26], where the precursor film is rapidly exposed to a solvent which poorly solvates the precursors and leads to the rapid nucleation of perovskite and almost complete surface coverage. This method can produce excellent film qualities but integrating this into a standard slot-die coating process is difficult. For these reasons many of the first reports of slot-die coated perovskite layers made use of the two-step method, as it can result in high surface coverage.

Schmidt et al. compared the effects of the two-step deposition with that of one-step on slot-die coated films [27]. The outcome of both approaches was found to be dependent on the device stack and interlayers the precursor solutions were deposited onto, the one-step deposition performed better with ITO/PEDOT: PSS (P-I-N 'inverted' architecture stack) geometry while perovskite would did not form on a ITO/ZnO/PCBM (N-I-P 'standard' architecture stack) geometry. The lower performance with one-step deposition in an N-I-P stack is linked to poor film coverage of the perovskite on top of the electron transport layer (ETL), leading to lower photocurrent [28]. Whereas for two-step deposition perovskite formation was achieved in both device stacks, however the performance of the P-I-N stack devices was very poor. This demonstrates the importance and interplay of the deposition process (one or two-step), the properties of the substrate layer the formulation is being deposited onto. The nucleation and crystallisation of the different precursor solutions in dependent on the substrate surface.

In the two-step deposition process it is important to have highly uniform PbI_2 films with high surface coverage, but also films that can be converted to perovskite readily. Contrary to spin coating, the slow drying of the slot-die coated films gives enough time for mass transfer and solvent flow to cause non-uniformity in the films[29]. Hwang K et al. reported the impact of slow drying on slot-die coated PbI_2 films in an effort to deposit the perovskite layer sequentially [16], the formation of highly non-uniform films upon slow drying was noticed, to mitigate the unwanted flow of the ink a process to mimic the spin coating drying mechanism by externally quenching the films by a gas jet was employed. A second slot-die coating head was connected beside the first head and compressed nitrogen gas was flowed on to the just deposited wet film, to speed drying, the 'gas quenched' PbI_2 films formed were found to be dense and with uniform film coverage. Figure 2 shows the difference in the PbI_2 film morphology with gas quenching to that of films allowed to dry under ambient conditions. The dense lead iodide films formed using this process were found to poorly convert to perovskite when exposed to MAI. To increase the reactivity of the PbI_2 films to MAI and obtain full conversion to perovskite, a solvent vapour soaking technique was employed. After drying the gas quenched PbI_2 films were stored in an enclosed chamber, this resulted in a more porous film that allowed complete penetration of MAI and a high degree of conversion to perovskite, as well as achieving good film coverage with few pin hole formations. As the perovskite layer, the ECL and hole transport layers (HTL) were deposited using slot-die coating, resulting in a hero cell performance for the complete slot-die coated device of 11.96% PCE. However, storing the film for long periods to make it more reactive is not an ideal method, especially for a scaled-up manufacturing process where reducing the production time and maximising throughput are critical, the process also limits the transition to continuous roll to roll fabrication.

In order to develop a more scalable method to produce highly reactive PbI_2 films the same group reported using a method, previously demonstrated for spin coated devices [30, 31], involving an unstable perovskite intermediate [18]. A non-

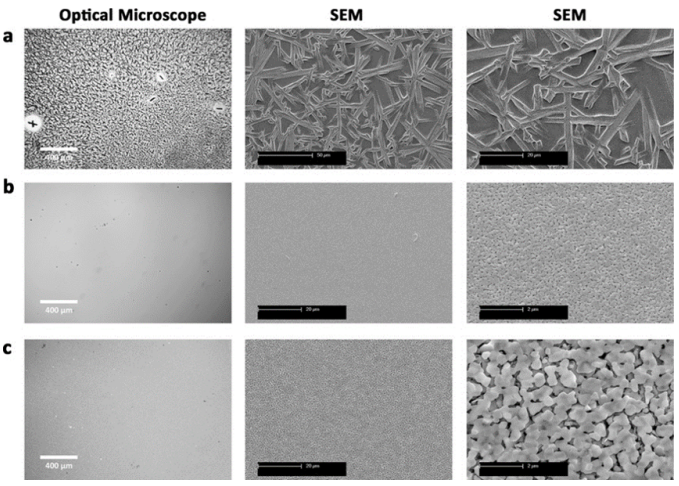

Figure 2: Optical microscopy and SEM images of the slot-die coated PbI_2 films by (a) ambient drying (b) gas-quenching and air storage (c) by gas quenching and enclosed space storage. Reproduced with permission from ref [16]. Copyright 2015, Wiley.

stochiometric amount of MAI (referred as intra-addive approach) was added to the PbI_2 formulation to slow down the PbI_2 crystallization in the first deposition step making it highly reactive at the second step, this subsequently gives greater conversion to the final perovskite. Figure 3 shows the schematic representation of the process. A PCE of 5.8% was achieved with a R2R processed device on a flexible substrate with evaporated top contacts. To push the PCE further, $CH_3NH_2PbI_3$ was replaced with the double cation perovskite ($FA_{0.4}MA_{0.6}PbI_3$) whereby 40mol% FAI was used as an additive in the first step along with PbI_2 followed by MAI deposition. This increased the PCE to 7.3% in the same device stack on a flexible substrate and led to a PCE of 11.0% when the P3HT hole transport layer (HTL) was changed to PEDOT:PSS, (see Figure 3). The similar approach was further used by Gong et al. to deposit triple cation perovksite [32]. The active layer was partially printed by microgravure printing. For the printing of active layer, PbI_2/CsI films with samll amount of MAI/FAI (as an intra additive) was first printed using microgravure method on top of gravure printed SnO_2. This was followed by slot die coating of FAI/MAI mixture for the complete conversion to perovskite. In additon, gas blowing was used to reduce the roughness of the perovksite film resulting in improved performance of the stack . Intra additive approach combined with gas blowing resulted in hero PCE of 10.57%.

Another method, 'mediator extraction treatment' (MET) for the preparation of PbI_2 films that result in high quality perovskite layers was reported by Kim et al. [33]. A PbI_2 ink formulation of lead iodide in Dimthylformamide (DMF) with 10%vol/vol Dimethyl sulfoxide (DMSO) was first slot-die coated, and then exposed to a gas flow from an air knife. This resulted in a PbI_2-DMSO complex, which was then dipped in an antisolvent bath to extract DMSO. In the following conversion step, the resulting PbI_2 films were dipped in a MAI bath (mixed with 25 wt% mehylammonium chloride), which once dried, converted to the final perovskite phase. The MET pro-

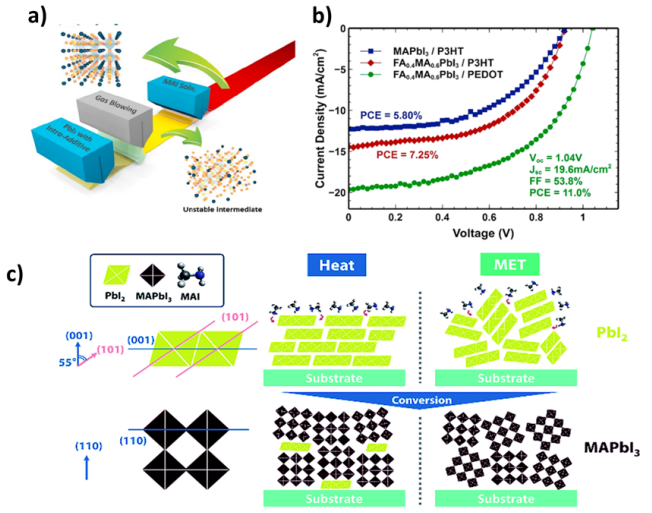

Figure 3: (a) Schematic illustration of the coating procedure (b) JV curve of the R2R coated devices. Reproduced with permission from ref [18]. Copyright Elsevier, 2017 (c) A schematic illustration showcasing the different PbI_2 crystal orientation made by MET and heat treatment and subsequent $CH_3NH_3PbI_3$ films. Reproduced with permission from ref [33]. Copyright 2018, Royal Society of Chemistry.

duced porous PbI_2 films with relatively randomized crystal orientation, giving a highly reactive PbI_2 film, a schematic representation of the crystal orientation is shown in Figure 3. The random orientation of crystal increased the MAI penetration rate within the PbI_2 films and subsequently led to conversion to perovskite within 100 seconds, this method produced a maximum PCE of 18.3% which was comparable to a spin coated active layer.

Yu-Ching Huang et al. reported the use of near infrared (NIR) heating for the drying of two-step perovskite films, for both the PbI_2 layer and the perovskite film when used in a P-I-N device structure with ITO coated glass substrate, PEDOT:PSS HTL and PCBM/PEI ETL and silver top electrode. This was combined with depositing the PbI_2 ink onto a heated substrate to improve the lead iodide film formation, The drying times of the perovskite layer was reduced from 1500 to 30s with the use of NIR heating [34].

As much as good stability and efficiency are priorities in a scaled-up photovoltaic manufacturing process, the safety of the process is equally important. In PSCs, the solvent and Pb are the main source of toxicity and significant efforts have been put towards low toxicity and green solvents for perovskite precursors. The sequential deposition route has also attracted interest due to the ability to use relatively non-toxic solvent systems, compared to the commonly used DMF solvent system. Remeika et al. demonstrated to use of low toxicity DMSO as a solvent for lead iodide formulations used for slot-die coating, although the layer was not optimised for performance and resulted in low PCEs [35]. Burkitt et al. developed an improved deposition method, again using DMSO as solvent for lead iodide, that resulted in improved film formation and device performance compared to those using DMF as solvent [36]. By also heating the m-TiO_2 coated substrate, to 100°C, then directly coating on to this, the PbI_2 films were made more reactive to MAI and to give greater levels of conversion to perovskite. The choice of solvent for the MAI ink was also optimised for slot-die coating and ethanol found to be the best of those assessed, this resulted in devices produced with slot-die coated PbI_2 and MAI with average PCEs of 11% and a hero PCE of 13.2%. In another work, the use of these solvent systems was further demonstrated in a R2R process, using a P-I-N device stack with ITO coated PET substrate, PEDOT:PSS HTL and PCBM/BCP ECL and silver top electrode, but the low volatility of the DMSO solvent led to reticulation of the PbI_2 film on drying in the R2R ovens. By increasing the drying temperature the film formation was improved, but this resulted in damage to the temperature sensitive substrate and a wide spread in device performance [21].

Two-step deposition has been shown to produce high efficiency small area devices, with PCEs up to 18.3% and been shown to work in R2R processes. Key to these results has been speeding the drying of the PbI_2 films to improve film uniformity and also using methods that result in films that react readily to form perovskite, either through enclosed chamber storage, mediator extraction treatment, solvent choice or intra-additive approaches. Of these the intra-additive approach has shown great potential for R2R processing and combined with the developments of MET and safer solvents along with rapid heating methods could deliver a viable R2R process for the slot-die coating of perovskite films.

2.2. *One-Step*

Due to the increased complexity, coating time and potentially lower yield, two-step deposition is not the ideal method for a scaled-up manufacturing process and a one-step process would be preferred. PSCs stacks can be broadly divided into two categories, N-I-P (standard) and P-I-N (inverted). Most of the work to date has reported one-step slot-die coated perovskite in the P-I-N geometry due to improved perovskite film coverage on top of an organic layer e.g. PEDOT:PSS. However, the stability of the P-I-N stack is a concern to commercial development [37]. PEDOT:PSS, the most commonly used HTL in an P-I-N geometry is vulnerable to water. The instability of the ITO/organic interface, the acidic nature of PEDOT and diffusion of PSS are additional reasons that makes this stack prone to faster degradation [38, 39]. But, unlike the N-I-P stack which normally requires high temperature sintering for the metal oxide layer, the P-I-N stack consists of organic layers which are processed at low temperatures and are therefore compatible with plastic substrates, hence are more easily R2R compatible. However, recent developments [40] in low temperature processed metal oxide electron transport layers like tin oxide (SnO_2) have created a route for N-I-P stacks to be compatible with plastic substrates, as discussed in more detail in Section 4.

2.2.1. *Controlling Film Formation Through Drying Conditions*

For one-step perovskite formulations the device stack of choice was initially the P-I-N, due to the improved film quality,

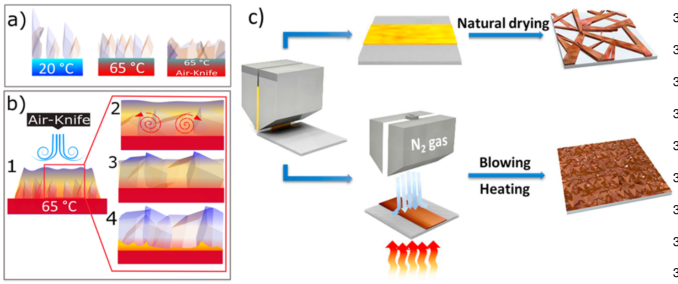

Figure 4: (a) Illustration of layer differences with varying conditions (b) 1. Use of air knife following initial nucleation growth. 2. Convective motions and reduced viscosity boost the crystal growth at the interface with the substrate 3. Crystals approach the cooler region reducing the vertical growth rate in favour of lateral growth across the warm substrate. 4. Reduced thickness is achieved. Reproduced with permission from ref [41]. Copyright 2016, Elsevier. (c) Schematic representation of the perovskite film formation via slot-die coating under the gas-blowing process combined with substrate heating. Reproduced with permission from ref [43]. Copyright 2018, Elsevier.

but many works developed novel strategies to improve the one-step film formation in the N-I-P stack. Cotella et al. demonstrated one-step deposition of $CH_3NH_3PbI_{3-x}Cl_x$ perovskite in DMF solvent system on a mesoporous titanium dioxide (m-TiO_2) metal oxide scaffold through a heating process and externally quenching the perovskite film, with an air-knife, to mimic the self-quenching step similar to spin coating. [41] By developing a temperature gradient, formed by heating the substrate, between the top and bottom of the wet film the suppression of the vertical growth of perovskite crystals was shown, Figure 4. This inherently forces horizontal perovskite crystal growth, thereby reducing the roughness of the film. Furthermore, adding the air knife treatment increases the temperature gradient by removing a greater proportion of energy from the top of the film and hence suppressing vertical crystal growth, leading to flattening of the films with relatively lower roughness, Figure 4. With the growth of a highly uniform film with high surface coverage, a PCE of 9.2% was recorded.

Following this work, the same group reported the deposition of four layers of the same device stack via slot-die coating, including the compact TiO_2 (titanium dioxide) metal oxide layer, the m-TiO_2 layer, the perovskite layer and the Spiro-OMeTAD HTL, further demonstrating the potential of slot-die coating for this device stack[42]

Following the work by Cotella et al., a similar approach was taken by Kim et al. to produce high quality $CH_3NH_3PbI_3$ perovskite films from a DMF solvent system in a one step deposition on planar N-I-P PSCs with a ZnO ETL. By combining blowing and heating of the film to speed nucleation and evaporation of solvent, the formation of large perovskite crystals with voids between was avoided and surface coverage and uniformity improved, resulting in a PCE of 12.7% [43]. Ciro et al. demonstrated flexible planar P-I-N stack PSCs using an ITO coated PET substrate, PEDOT:PSS HTL, $CH_3NH_3PbI_{3-x}Cl_x$ perovskite from DMF solvent system and PCBM ETL [44]. To improve the morphology of the perovskite film the solids content of the formulation was optimised along with heating of the substrate (to an optimal temperature of 80°C, which resulted in both improved surface coverage and lower surface roughness. Although the absolute PCEs were low, this nonetheless demonstrated substrate heating and drying conditions as an effective way to control perovskite film morphology.

Attempts to control perovskite film formation using drying methods have shown that increasing the nucleation rate of the perovskite film is important for achieving films with high surface coverage and that rapid drying of the solvent can help to avoid the formation of large crystallites and voids within the film.

2.2.2. *Controlling Film Formation Through Precursor Choice*

Rapid crystallization was also implemented by Lee et al., in a P-I-N stack with PEDOT:PSS HTL and C_{60}/PCBM ETL, using mixed lead precursors in a DMF solvent system, the use of mixed lead acetate and lead chloride precursors in the perovskite ink was demonstrated[45]. Lead acetate induces fast crystallization by forming an unstable organic by-product (methylammonium acetate) [46]. The use of lead acetate as the only Pb source combined with gas blowing however, caused the rapid crystallization on the surface of the film. This then entrapped the remaining solvent and by-product within the film, causing the formation of voids in the active layer. To avoid this, lead chloride was added alongside lead acetate to retard the rapid crystallization on the surface, avoiding any formation of voids, Figure 5. Using two different lead anion precursors combined with gas blowing improved the grain size, morphology and film coverage and resulted in a PCE of 13.3% over a small area of 0.1 cm^2 and 8.3% PCE over a 10cm^2 module.

Similar use of lead acetate was made by Kamaraki et al. on flexible ITO coated PET substrates, with slot-die coated PEDOT:PSS HTL and PCBM ETL layers also, using a solely lead acetate precursor in DMF solvent system [47]. The deposition temperature of the perovskite ink was optimised and similar to the work of Ciro et al. [44] resulted in changes in surface roughness. Optimised coating conditions for all three layers resulted in average PCEs of 5% and a maximum of 6.5%. Notably, Giacomo et al. also used a mixed lead chloride and lead acetate precursor solution in DMF for large area high performance module fabrication in a nitrogen atmosphere glove-box system [48].

Judicious selection of perovskite precursors is another method to control the nucleation and crystallization rate of perovskite films and so improve surface coverage and morphology. When this is combined with methods to control the drying of the films it can result in high performance cells and modules.

2.2.3. *Controlling Film Formation Through Solvent Choice*

Jung et al. demonstrated the use of solvent additives for refining the morphology of one-step slot-die coated $CH_3NH_3PbI_3$ perovskite films in a P-I-N device stack with PEDOT:PSS HTL and PCBM ETL [49]. 5vol% of N-cyclohexyl-2-pyrrolidone (CHP) along with 6vol% of dimethyl sulfoxide (DMSO) was mixed in with the 0.75M perovskite DMF solvent system precursor ink. Fourier-transform infrared spectroscopy (FTIR) results showed adduct formation between PbI_2 and DMSO and that this was dominant over that with DMF and CHP. The high polarity and high basicity of DMSO compared to that of DMF

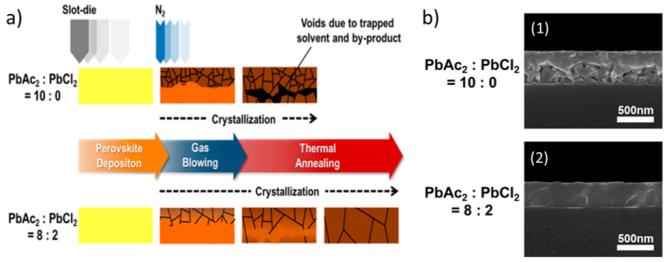

Figure 5: (a) Schematic representation of the crystallization of perovskite films. (b) SEM images showcasing the voids formed by rapid crystallization of perovskite and the same being mitigated by addition of $PbCl_2$. Adapted with permission from ref [45]. Copyright 2018, American Chemical Society.

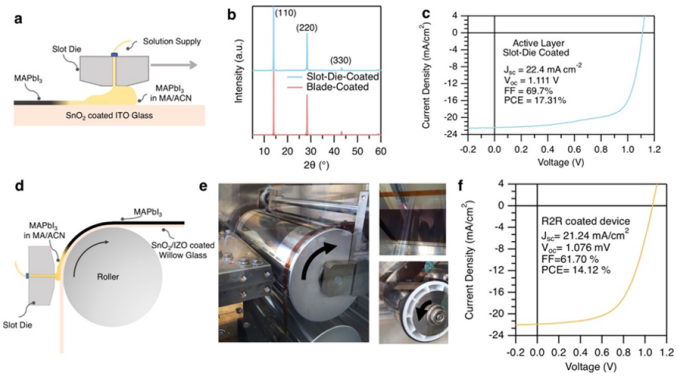

Figure 6: (a–c) Schematic illustration of slot-die coating process on rigid substrate (a) XRD (b) JV data (c). (d) Schematic illustration of slot-die coating process on flexible glass substrate with R2R process. (e) Images showing R2R coating (f) JV curve of the best performing R2R-coated device. Adapted with permission from ref [20]. Copyright 2018, American Chemical Society.

and CHP were found to be the reason for this behavior. The adduct formation with DMSO mainly retarded the crystallization rate of perovskite films. Interestingly CHP having the high boiling point and low vapour pressure likely remained in the solidifying film and assisted in uniform nucleation growth. Together the combined effects of these result in uniform and homogenous perovskite films that consequently resulted in better performance. Moreover the binary additive was found to play a role in preferentially oriented crystal growth of perovskite films which again helped in better charge transport [50].

PCEs of around 18% with slot die coating have been achieved by making use of DMF and N-Methyl-2-Pyrrolidone (NMP) [33, 51].However, the high toxicity of DMF and NMP limits its usage in manufacturing process. A safer alternative was developed by Noel et al. wherein the composite of acetonitrile (ACN) with methylamine gas was developed to dissolve MAI and PbI_2 [52]. Due to the low boiling point and high volatility of ACN, 98% of crystallization was noted (after ˜110 sec) at room temperature. The rapid crystallization of the ACN based formulation and lower toxicity, relative to DMF, fit well into the criteria for its use in large area fabrication and the low viscosity potentially means high slot-die coating speeds can be attained. Dou et al. implemented this formulation for slot-die coating, in a R2R fabrication process using a flexible indium zinc oxide coated glass substrate and a N-I-P device stack, with slot-die coated tin oxide ETL [20]. The optimized R2R process led to the formation of uniaxially oriented crystalline smooth perovskite films. A hero PCE of 14.12% was reported for R2R and 17.31% for S2S slot-die coated films, Figure 6. While the ACN formulation is suitable for large area deposition, it could be argued that high flammability and still considerable toxicity of this solvent system might hinder its commercial use.

Alternatively, DMSO is another less toxic solvent for use in large area manufacturing of PSCs. The solvent itself is considered low toxicity but it is able to easily penetrate the skin along with any solute dissolved in it. However, with proper safety precautions it is an attractive option. Unfortunately, the poor wetting of DMSO on most substrates makes it quite difficult to print with good film coverage. Galagan et al. demonstrated the addition of 10%vol/vol 2-Butoxyethanol in DMSO to lower the surface tension of the solvent mixture. This improved wetting and achieved improved film coverage [19]. In a R2R process, using a flexible ITO coated PET substrate and N-I-P device stack, using a slot-die coated tin oxide layer and a slot-die coated $Cs_{0.15}FA_{0.85}PbI_{2.85}Br_{0.15}$ perovskite layer the best performing device demonstrated a PCE of 15.2% over an active area of 0.09cm^2 and a stabilised PCE of 13.5%.

Modification of solvent systems offers a powerful tool to control the perovskite film morphology and has resulted in high performance R2R devices, but careful consideration needs to be given to the suitability of such systems for industrial manufacture.

2.2.4. *Controlling Film Formation Through Additives and Surface Modification*

Additives have played a large role in improving the stability and efficiency of PSCs by influencing crystal growth and the morphology of perovskite films [53]. Zuo et al. used a NH_4Cl additive to improve the perovskite film quality in a $CH_3NH_3PbI_3$ perovskite formulation in DMF with small additions of NH_4Cl using a P-I-N device stack with PEDOT:PSS HTL and PCBM ETL [17]. Absorption spectroscopy confirmed the higher absorption of light by the active layer in the presence of NH_4Cl. Additionally higher photoluminescence intensity was observed in the films with NH_4Cl, confirming mitigation in non-radiative recombination and film defects. For slot-die coated devices the use of a NH_4Cl additive was combined with heating of the substrate and gas blowing, yielding high-quality perovskite films for both S2S glass substrate devices and R2R devices on flexible PET substrate. Notably the fabrication was carried out at 45% relative humidity demonstrating a hero cell performance of 15.57% PCE for S2S coated devices and 11.16% PCE with R2R coated devices.

A different approach to improve perovskite film morphology and reduce defects is by surface treating interlayers. In one such work, by Gu et al., 3-aminopropanoic acid as an ambipolar self-assembled monolayer (C3-SAM) was introduced for the modification of PEDOT:PSS [54]. Using a P-I-N device stack with $CH_3NH_3PbI_{3-x}Cl_x$ perovskite formulation, PEDOT:PSS HTL and PCBM/ZnO ETL, C3-SAM was applied to the PEDOT:PSS film. The modified PEDOT:PSS helped in better perovskite film

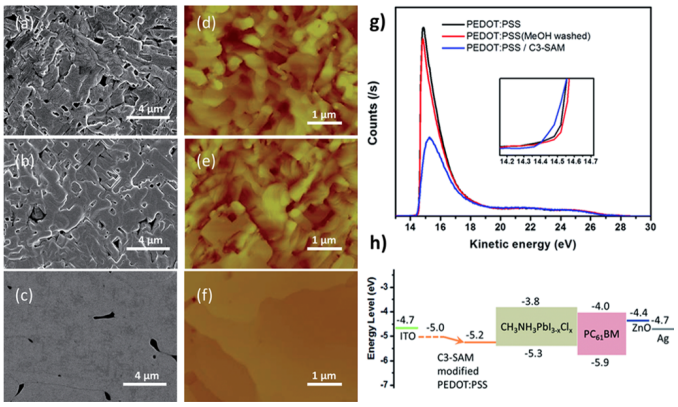

Figure 7: SEM (a–c) and AFM (d–f) images of $CH_3NH_3PbI_{3-x}Cl_x$ films on the as-prepared PEDOT:PSS (a and d), methanol washed PEDOT:PSS (b and e) and C3-SAM modified PEDOT:PSS (c and f). (g) The ultraviolet photoelectron spectroscopy (UPS) spectra of the as-prepared PEDOT:PSS (black line), methanol washed PEDOT:PSS (red line) and C3-SAM modified PEDOT:PSS (blue line). (h) The energy band alignment of PSCs. Reproduced with permission from ref [54] Copyright 2015, Royal Society of Chemistry.

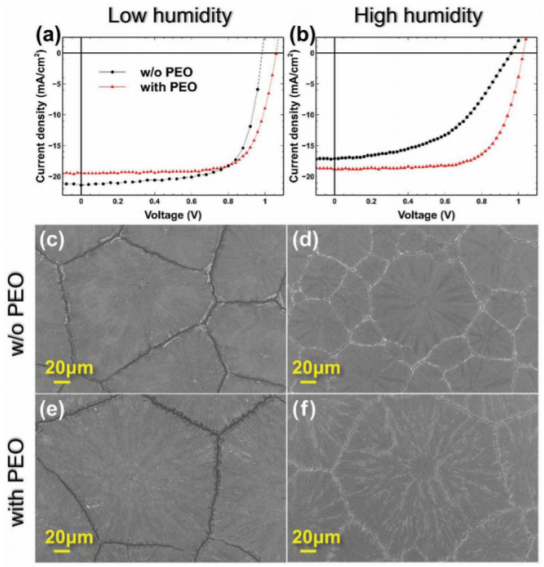

Figure 8: Comparison of device performance and surface morphology with and without PEO at in a low (30±5% RH) and high (55±5% RH) humidity coating environment. JV curves of the slot-die coated devices in (a) low and (b) high humidity, SEM images of perovskite films on glass/ITO/m-PEDOT:PSS substrates w/o PEO deposited in (c) low and (d) high humidity, and with PEO deposited at (e) low and (f) high humidity. Reproduced with permission from ref [55]. Copyright 2019, Wiley.

growth but also had a positive effect on the energy band alignment by inducing an extra permanent dipole. It was further confirmed by UV photoelectron spectroscopy, that the treatment of C3-SAM lowered the work function of PEDOT:PSS by 0.2eV, Figure 7, the improvement in charge transport and film morphology led to the hero PCE of 5.1% on flexible S2S roll coated PSCs.

Recently, Kim et al. introduced polyethylene oxide (PEO) as an additive in slot-die coated perovskite films, using a P-I-N stack with modified PEDOT:PSS HTL, $(CH_3NH_3)_{0.6}(HC(NH_2)_2)_{0.38}Cs_{0.2}PbI_{2.975}Br_{0.025}$ and PCBM/PEIE ETL and evaporated Ag top electrode [55]. This was used in conjunction with using $PbCl_2$ as the source of chloride as an additive and with deposition of the perovskite ink onto a heated substrate. The polymer additive was found to improve the tolerance of perovskite to deposition in high humidity (approx. 55% RH) conditions and resulted in clear changes to performance, Figure 8. This novel method for the fabrication of PSCs in ambient conditions has the potential of driving manufacturing cost further down, an important step towards commercialization. Notably it's the only fully R2R (except top contact) processed PSC reported so far, showing an impressive efficiency of 11.7%.

3. 2D Perovskite Layers

Recently, 2D perovskites have gained interest due to improved lifetime compared to 3D perovskites [56]. 2D perovskites are typically prepared by introducing a large organic molecule (for example butylammonium) in between the layers of 3D perovskite. Previously the performance of the PSCs with 2D perovskite have been quite low compared to 3D perovskite, however they have significantly improved in the past few years and have recently achieved 14.1% PCE [57]. Excellent lifetime and improvement in the performance of 2D perovskite based PSCs has encouraged their use with large area printing and coating techniques. Fu et al. first demonstrated R2R printed 2D perovskite reporting an impressive PCE of 8% on plastic substrate and 12.5% by batch coating on glass substrate [58]. Loss in performance in the R2R printed device compared to spin coated device (14.9% PCE) was attributed to mediocre film quality by R2R slot-die deposition due to less hydrophilic surface of ITO/PET. However, it is an encouraging report with the first ever R2R coated 2D perovskite and shows progress for large area 2D perovskite PSCs.

4. Interlayers

Although it is important to perfect the deposition of the perovskite layer, it is also vital to achieve the same with charge transport layers. Defects in the coatings can be detrimental to device performance through various processes; voids and pinholes can cause shunt leakages and lead to shorts, poor charge blocking capabilities can lead to increases in recombination of charge carriers. In addition to this, temperature limitations must be overcome for coating onto temperature sensitive substrates such as PET, where a maximum processing temperature of 140°C is required. This significantly hinders the deposition of the more common solution processed ETLs such as; tin oxide (SnO_2) from tin chloride ($SnCl_4.2H_2O$) [59], NiOx from nickel (II) acetate tetrahydrate, and TiO_2 from titanium diisopropoxide bis (acetylacetonate) [60], which require much higher annealing temperatures of 300°C and above.

4.1. Tin Oxide Electron Transport Layer

Tin oxide (SnO_2) has gained significant usage as an ETL in perovskite devices, due to its high electron mobility, better band alignment with perovskite when compared to TiO_2 and unlike TiO_2 it doesn't induce serious UV degradation [40]. Therefore, SnO_2 is a strong candidate for an ETL in devices in terms of both performance and stability. The use of SnO_2 is well established in small area devices, with the majority of reports employing a tin (IV) chloride precursor [40, 59]. Although this precursor requires a relatively low temperature anneal at 180°C, it is still too high to be compatible with common flexible substrates e.g. PET, in addition a long annealing time of around one hour is required.

Recently the use of SnO_2 formulations for low-temperature R2R depositions with excellent device performance have been reported. Galagan et al. [19] and Bu et al. [61] used a colloidal suspension of tin (IV) oxide 15% wt./vol in H_2O (Alfa Aesar), which can be dried at 140 - 150°C in a shorter period of time. Galagan et al. employed this SnO_2 solution into a R2R N-I-P stack, in which the solution was diluted with 10vol% 1-butanol to aid wetting and slot-die coated at 5m/min, with subsequent drying at 140°C in a 20m length oven at the same speed. Perovskite was also R2R coated, with the subsequent spiro-OMeTAD and gold contacts deposited offline, achieving a hero cell reverse scan PCE of 15.2% and a stabilised PCE of 13.5%. Bu et al. also used this SnO_2 solution for use in bench-top S2S slot-die coating for devices and modules on ITO coated PET substrate. The colloidal suspension was diluted with IPA in a 1:1 ratio to aid in the wetting of the ink on the substrate. Three slot-die coatings of the ink were made to build up the film thickness and improve uniformity, followed by drying at 140°C for 60 minutes. Such a long drying time is unattractive for high throughput R2R coating, however, Galagan et al. showed that this drying time can be reduced to a few minutes. Bu et al. highlighted the fact that the KOH stabilizing agent in the SnO_2 solution also passivates the perovskite/SnO_2 interface leading to enhanced efficiency and stability. The rest of the device stack in this case was spin-coated but does however prove the compatibility of this SnO_2 solution with a slot-die coating process capable of producing high efficiency devices and modules with PCEs of 17.18% for small area devices and an impressive 15% for a 5 x 6 cm^2 flexible module.

4.2. Zinc Oxide Electron Trasport Layer

Slot-die coated Zinc Oxide (ZnO) layers have been widely used in organic photovoltaic devices [62]. Hwang K et al. used this knowledge and made a fully R2R coated perovskite device, apart from evaporated contacts, using a ZnO nanoparticle solution made in house [16]. No difference was noted when comparing the slot-die coated zinc oxide to the spin coated equivalent. Slot-die coated zinc oxide layers required a relatively short drying time of 10 minutes at 120°C, demonstrating compatibility with a R2R processes on temperature sensitive substrates. However, zinc oxide has been reported on numerous occasions to cause stability problems with perovskite devices and induce rapid degradation of the perovskite layer. It is well reported that thermal annealing of perovskite on top of ZnO causes the perovskite to decompose and is due to the basic properties of the ZnO, causing deprotonation of the methyl ammonium cations.

Krebs et al. also used low-temperature (110°C) dried, slot-die coated ZnO on flexible ITO coated PET substrates with N-I-P device stack, with a PCBM interlayer between the ZnO and perovskite [27]. Krebs et al. also found that annealing the perovskite precursor on top of the ZnO caused issues with perovskite formation, and overcame this by using a two-step perovskite deposition, which gave a champion efficiency of 2.6%. Although the device performance is relatively low due to the use of a printed top electrode, it does demonstrate the compatibility of ZnO in a R2R compatible process.

The instability of ZnO based devices can, to an extent, be reduced by depositing the ZnO on top of the perovskite, usually using a nanoparticle formulation, firstly by negating the need for thermal annealing of the perovskite on the ZnO surface, and secondly as ZnO has a strong resistance to oxygen and humidity [63].

4.3. Titanium Dioxide Electron Transport Layer

Slot-die coating of the TiO_2 blocking layer has been achieved by Burkitt et al., but required sintering at 550°C for an extended period, which is not low-temperature substrate compatible. In order to achieve an adequate blocking layer the solvent system for the titanium diisopropoxide bis (acetylacetonate) precursor was optimised and two coatings of the layer made, one on top of the other in an attempt to fill pin-holes and coating defects [42]. More recently Hossain et al. have reported the use of TiO_2 nanoparticles for a low-temperature coatable blocking layer processed at 100°C. As the nanoparticles are pre-synthesised in the anatase phase, high temperature annealing is avoided. Using these nanoparticles Hossain et al. achieved a stabilised efficiency of 15.7% using slot-die coating or alternatively the same efficiency was achieved using inkjet printing of the layer, demonstrating the potential for low temperature TiO_2 slot-die coating formulations [64].

4.4. Hole Transport Layers

Slot-die coating of HTLs in PSCs has been reported for both P-I-N and N-I-P device stacks. For the P-I-N stack the most common of these is PEDOT:PSS, the slot-die coating of which has been well developed for organic photovoltaics; modified PEDOT:PSS layers for slot-die coating have been reported [17, 65] to improve the energy level alignment with perovskite, but nonetheless PEDOT:PSS is still seen as an unattractive HTL due to stability issues. Zuo et al. reported on slot-die coating of reduced graphene oxide as a replacement for PEDOT:PSS that resulted in improved performance and could be a potentially attractive HTL for large area PSCs [17, 66]. Metal oxide HTLs, such as nickel oxide (NiOx) are seen as potentially more stable alternatives to PEDOT:PSS and in a conference proceeding report from Giacomo et al. slot-die coating of NiOx was reported, but a comprehensive explanation of the processing conditions has not yet been given [67].

For the N-I-P device stack slot-die coating of spiro-MeOTAD was reported by Burkitt et al. [42] where the use of a highly

toxic chlorobenzene solvent system was avoided by replacing this with less toxic toluene, but the stability issues of spiro-OMeTAD are still unattractive for the use of this HTL in large area depositions. Qin et al. reported the replacement of spiro-MeOTAD with bifluo-OMeTAD, that forms amorphous films and avoids the formation of large crystallites that worsen the performance of spiro-OMeTAD films, this resulted in a high performance of 14.7% PCE for devices with slot-die coated ETL, perovskite and HTL.

The use of P3HT as a slot-die coated HTL has also been reported for both S2S and R2R devices, but has generally resulted in lower performance or been used in conjunction with another evaporated HTL [16, 18].

Slot-die coating of HTLs is a relatively understudied area of research and in particular the reports on the deposition of more stable materials and metal oxides is scarce.

5. Contacts

In PSCs transparent conductive oxides (TCO) have been the preferred choice for transparent electrode (hereafter referred as bottom electrode) mainly because of its good electrical conductivity and high transparency. TCOs are widely used across several industries for various applications like smart windows, touchscreens, organic light emitting diodes, liquid crystal displays and antistatic coatings. Given their commercial use, they have been well optimized for large scale production. However, they still contribute to over 70% of the total cost of PSCs. Looking at alternatives, Sears et al demonstrated TCO free slot die printed transparent electrode for PSCs by replacing tin doped indium oxide by Ag/PEDOT:PSS achieving PCE of 11%.[68].

For top contact, high vacuum thermal evaporation is typically used for lab scale fabrication which basically is a bottle neck for cost effective high through put manufacturing. Printing the solution processed top electrode is not trivial for number of reasons. Ideal top electrode would have high conductivity which can be processed at low temperature and the processing solution must be orthogonal to all the layers underneath. To realize complete solution processed PSCs, solutions like fully printed mesoscopic PSCs[10] and printable top electrodes have been proposed.[69]. However, till date to the best of our knowledge no reports are available showcasing the slot die printing of top electrode in PSCs. Other techniques like ink-jet [70] and spray coating[69] have been implemented to print silver nanowire as top electrode.

6. Module Representation

Good performance has been reported so far on slot-die coated PSCs, however, this has been demonstrated mostly for small area devices with small aperture masks used for testing. It is equally important to showcase the performance of large area printed PSCs to assess its potential for manufacture and actual power generation. The first slot-die coated perovskite module was reported by Hwang K et al. with 40cm^2 active area but the performance was poor and not reported fully [16]. Later in 2018, Lee et al. reported the use of mixed Pb precursors, Section 2.2.2, for the fabrication of large area PSCs. This strategy was successfully implemented for module fabrication attaining 8.3% PCE on 10cm^2 area [45], it is to be noted that only perovskite was printed via slot-die coating in this report. Following this, Giacomo et al. demonstrated a module, Figure 9, with PCE of 10% on a 6-inch substrate with an active area of 168.75cm^2, notably the one-step perovskite and HTL were both printed by slot-die coating while the ETL was deposited by electron beam deposition [48].

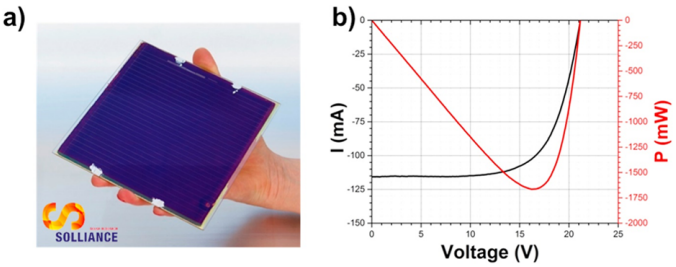

Figure 9: (a) – 6 in. by 6 in. perovskite module; (b) – IV curve and power curve of the 6 in. by 6 in. module, with the actual module dimension of 168.75 cm^2, containing 25 interconnected cells. Reproduced with permission from ref [48]. Copyright 2017, Elsevier.

7. Outlook and Perspectives

Slot-die coating has proven to be a powerful tool for the deposition of perovskite films for both high performance small area devices and large area modules, it is also one of the only techniques to have been used for the demonstration of R2R fabrication of perovskite solar cells. A great deal of effort has been directed at developing strategies for controlling the formation of the perovskite layer, both in terms of achieving a high rate of nucleation to facilitate the formation of films with high surface coverage and in controlling the crystallisation and crystal growth of the perovskite to achieve large grain sizes with good interconnection and orientation. These have been achieved using a variety of methods including drying regimes, precursors and additives, surface modifications and solvent systems, as well as by separating the perovskite deposition process out into multiple steps. In most cases combinations of these methods have been combined and adapted to the particular set of processing conditions used.

To date the two most promising slot-die perovskite methods reported are the R2R demonstrations from Dou et al. [20] and Galagan et al. [19]. The use of the ACN:MA solvent system in the work of Dou et al. demonstrates the great potential of this system for the easy deposition of high quality perovskite films that dry rapidly and are deposited from a low viscosity solvent system. But, along with the toxicity of ACN the other downside to this system is that it has been reported that caesium ions show poor solubility in this system and Cs containing perovskites have been reported as some of the most stable and high performing perovskites. The work of Galagan et al. demonstrates the potential for the deposition of mixed cation and anion perovskites, in particular containing caesium and the use

of lower toxicity solvent systems based on DMSO, but DMSO is relatively low volatility and achieving good film formation and rapid drying is not trivial. Both works show great promise for the development of slot-die coating fabrication methods and finding ways to achieve the best of both in one system seems a highly desirable target. In particular, achieving a rapid drying low viscosity solvent system that is also able to deliver Cs ions but avoids the use of toxic ACN would overcome some of the hurdles to demonstrating a reliable industrially relevant R2R coating process.

Both of these works have also shown the use of SnO_2 ETLs, deposited by slot-die coating, the work of Dou et al. using a higher temperature process and the work of Galagan et al. demonstrating the use of a lower temperature process. SnO_2 appears to be a clear leader for the development of slot-die coatable ETL formulations, using low cost precursors that require low deposition temperatures and result in high performance and stable devices. Further developing SnO_2 formulations to improve both the coating properties and electronic properties of the films is a sound progression for ETL development. Deposition of HTLs using slot-die coating is an under explored area and worthy of further study, the coating method seems well adapted to this and is likely to be the method of choice for R2R compatible coatings of these materials seen in the future. Slot-die coating has potential for deposition of other layers in the device stack, such as transparent conductive films and electrodes, but the lack of full 2D patterning might limit this to certain device stacks. As well as photovoltaics there are other technologies where slot-die coating of perovskites has been reported, including photodetectors [71] and PeLEDs [72] and developments in these areas are likely to also be relevant to photovoltaics.

8. Acknowledgements

This work was supported by the Engineering and Physical Sciences Research Council (EPSRC) through SPECIFIC Innovation and Knowledge Centre (EP/N020863/1 and EP/P030831/1). This project has received funding from the European Union's Horizon 2020 research and innovation programme under the Marie Sklodowska-Curie grant agreement No 764787. The authors would like to acknowledge the financial support provided by the M2A that has been made possible through funding from the European Social Fund via the Welsh Government, the Engineering and Physical Sciences Research Council (EP/L015099/1) and Tata Steel Europe that has made this research possible.

No.	Type	Device Stack	Key Concept	Scan Direction	Active Area (cm^2)	Voc (V)	Jsc ($mAcm^{-2}$)	FF (%)	PCE (%)	Stabilised PCE (%)	Hero PCE (%)	Refere
1.	S2S	PET/ITO/**ZnO/PCBM/$CH_3NH_3PbI_3$/P3HT/PEDOT:PSS**/Ag	Comparison of one and two-step methods	NS	0.2-0.5	0.69	4.6	47	1.6	NS	2.6	[27]
		PET/ITO/**PEDOT:PSS/$CH_3NH_3PbI_{3-x}Cl_x$/PCBM/ZnO**/Ag		NS	0.2-0.5	0.88	7.9	49	3.4	NS	4.9	
2.	S2S	Glass/ITO/**ZnO/$CH_3NH_3PbI_3$/P3HT**/Ag	Lead iodide film formation	NS	0.1	0.95	19.9	54	10.1	NS	11.96	[16]
3.	S2S	PET/ITO/**PEDOT:PSS/$CH_3NH_3PbI_{3-x}Cl_x$/PCBM**/Au	Substrate Heating	Reverse	0.12	0.68	9.6	33	2.4	NS	2.91	[44]
4.	S2S	Glass/FTO/c-TiO_2/m-TiO_2/**$CH_3NH_3PbI_{3-x}Cl_x$**/Spiro-OMeTAD/Au	Heated substrate and air-knife	Reverse	0.062	0.78	14.9	66	7.0	8.1	9.2	[41]
5.	S2S	Glass/ITO/**PEDOT:PSS/$CH_3NH_3PbI_3$/PCBM**/BCP/Ag	Solvent additives	NS	0.1	*0.87*	*14.3*	*77*	*9.57*	NS	*9.57*	[49]
		Glass/ITO/**FrGo/$CH_3NH_3PbI_3$/PCBM**/BCP/Ag		NS	0.1	*1.0*	*16.3*	*76*	*12.52*	NS	*12.52*	
6.	R2R	PET/ITO/**ZnO/$CH_3NH_3PbI_3$/P3HT**/MoO_3/Ag	Intra-additive sequential deposition	NS	0.1	*0.93*	*12.3*	*51*	*5.80*	NS	*5.80*	[18]
	R2R	PET/ITO/**ZnO/$(CH_3NH_3)_{0.6}(HC(NH_2)_2)_{0.4}PbI_3$/P3HT**/$MoO_3$/Ag	Mixed cations	NS	0.1	*0.93*	*14.4*	*54*	*7.25*	NS	*7.25*	
	R2R	PET/ITO/**ZnO/$(CH_3NH_3)_{0.6}(HC(NH_2)_2)_{0.4}PbI_3$/PEDOT:PSS**/$MoO_3$/Ag		NS	0.1	*1.04*	*19.6*	*54*	*11.0*	NS	*11.0*	
7.	S2S	Glass/FTO/SnO2/**$CH_3NH_3PbI_3$**/Spiro-OMeTAD/Au	Mediator Extraction Treatment	Reverse	0.096	*1.11*	*21.9*	*76*	17.3	NS	*18.3*	[33]
8.	S2S	Glass/ITO/SnO_2/**$CH_3NH_3PbI_{3-x}Cl_x$**/Spiro-OMeTAD/Au	Solvent and precursor additives	Reverse	0.06	*1.1*	*21.5*	*76*	*18.0*	15.6	*18.0*	[51]
9.	S2S	PET/ITO/**ZnO/$CH_3NH_3PbI_3$/P3HT**/Au	Surface treatments	Reverse	1.0	NS	NS	NS	1.6	NS	3.6	[35]
10.	S2S	PET/ITO/modified-PEDOT:PSS/**$CH_3NH_3PbI_{3-x}Cl_x$**/PCBM/Ca/Al	Use of NH_4Cl additive	Reverse	0.1	*1.02*	*19.8*	*77*	*15.57*	15.17	*15.57*	[17]
	R2R	PET/ITO/**modified-PEDOT:PSS/$CH_3NH_3PbI_{3-x}Cl_x$**/PCBM/Ca/Al		Reverse	0.1	*0.98*	*17.4*	*65*	*11.16*	NS	*11.16*	
11.	S2S	Glass/ITO/PEDOT:PSS/**$CH_3NH_3PbI_{3-x}Cl_x$**/PCBM/BCP/Ag	Mixed lead precursors	NS	0.1	0.88	16.6	78	11.4	NS	13.3	[45]
		4 cell module with same structure			10.0	*3.8*	*4.1*	*52*	*8.3*	NS	*8.3*	
12.	S2S	Glass/FTO/**c-TiO_2/m-TiO_2/$CH_3NH_3PbI_{3-x}Cl_x$/Spiro-OMeTAD**/Au	Four layers in N-I-P stack slot-die coated.	Reverse	0.09	0.8	15.8	46	5.73	7	11.9	[42]
13.	S2S	Glass/ITO/ZnO/**$CH_3NH_3PbI_3$**/Bifluo-OMeTAD/Ag	Blowing and heating of perovskite film	Reverse	0.1	*1.10*	*17.21*	*67.25*	11.10	NS	12.73	[43]
14.	S2S	Glass/ITO/TiO2/**$CH_3NH_3PbI_{3-x}Cl_x$/Spiro-OMeTAD**/Au	Large area module	NS	0.09	1.03	22.1	74	16.8	14	16.8	[48]
		25 cell module with same structure.		NS	151.87*	*21.2*	*17.3*	*68*	*11.1*	NS	*11.1*	
15.	S2S	Flexible Glass/IZO/**SnO2/$CH_3NH_3PbI_3$**/Spiro-OMeTAD/Au	ACN:MA solvent	Reverse	0.15	*1.11*	*22.4*	*70*	*17.31*	15.6	17.31	[20]
	R2R	Flexible Glass/IZO/**SnO2/$CH_3NH_3PbI_3$**/Spiro-OMeTAD/Au		Reverse	0.15	*1.08*	*21.2*	*62*	*14.12*	NS	14.12	
16.	S2S	Glass/FTO/c-TiO_2/**m-TiO_2/$CH_3NH_3PbI_3$**/Spiro-OMeTAD/Au	PbI_2 in DMSO	Reverse	0.09	0.96	16.7	67	11.0	NS	13.2	[36]
				Forward	0.09	0.95	15.2	59	8.7	NS	10.6	
17.	R2R	PET/ITO/**SnO2/$Cs_{0.15}(HC(NH_2)_2)_{0.85}PbI_{2.85}Br_{0.15}$**/Spiro-OMeTAD/Au	Mixed cation and DMSO with 2-butoxyethanol	Reverse	0.09	*1.03*	*20.7*	*72*	*15.2*	*13.5*	15.2	[19]
				Forward	0.09	*0.97*	*20.0*	*61*	*11.9*	*13.5*	11.9	
18.	S2S	Glass/ITO/PEDOT:PSS/**$CH_3NH_3PbI_3$**/PCBM/PEI/Ag	NIR heating	NS	0.3	0.98	18.4	67	12.0	NS	12.3	[34]
19.	R2R	PET/ITO/**m-PEDOT:PSS/$(CH_3NH_3)_{0.6}(HC(NH_2)_2)_{0.38}Cs_{0.2}PbI_{2.975}Br_{0.025}$/PCBM/PEIE**/Ag	PEO additive	Reverse	0.1	0.93	20.3	45	8.62	NS	11.67	[55]
20.	S2S	PET/ITO/**PEDOT:PSS/$CH_3NH_3PbI_3$/PCBM**/Ag	Pb precursor	Forward	0.1	0.96	15.9	35	5	NS	6.5	[47]
21.	S2S	PET/ITO/**PEDOT:PSS/C3-SAM/$CH_3NH_3PbI_{3-x}Cl_x$/PCBM/ZnO**/Ag	Surface modification	Forward	0.05	*0.98*	*13.7*	*38*	*5.1*	NS	*5.1*	[54]
22.	S2S	Glass/ITO/PEDOT:PSS/**$(CH_3(CH_2)_3NH_3)_2(CH_3NH_3)_3Pb_4I_{13}$**/PCBM/PEIE/Ag	2D Perovskite	Forward	0.1	*1.06*	*16.6*	*71*	*12.5*	NS	*12.5*	[58]
	R2R	PET/ITO/**PEDOT:PSS/$(CH_3(CH_2)_3NH_3)_2(CH_3NH_3)_3Pb_4I_{13}$**/PCBM/PEIE/Ag		Forward	0.1	*1.02*	*13.6*	*58*	*8.0*	NS	*8.0*	
23.	R2R	PEN/ITO/SnO_2/PbI_2-CsI/**$HC(NH_2)_2$I-CH_3NH_3I**/Spiro-OMeTAD/Ag	Two step mixed cation	NS	0.07	*0.98*	*16.82*	*64*	9.97	9.8	10.57	[32]

Table 1: Device stacks and JV scan photovoltaic parameters of slot-die coated perovskite devices reported in the literature so far.

Note:

1. Bold font indicates slot-die coated layer in the device stack.
2. The performance parameters (Voc, Jsc, FF and PCE) are the average values. Italic font is used if the mean values were not available and represents the parameters of hero cell and not mean values.
3. * The active area was calculated by multiplying the geometric fill fcator with that of substrate area.
4. R2R is a process involving transfer of substrates between two moving rolls. Therefore reports using just rollers, essentially roll coating are also termed as S2S.

References

[1] A. Kojima, K. Teshima, Y. Shirai, T. Miyasaka, Organometal halide perovskites as visible-light sensitizers for photovoltaic cells, Journal of the American Chemical Society 131 (2009) 6050–6051. URL: https://doi.org/10.1021/ja809598r. doi:10.1021/ja809598r. arXiv:https://doi.org/10.1021/ja809598r, pMID: 19366264.

[2] Best research-cell efficiency chart, https://www.nrel.gov/pv/assets/pdfs/best-research-cell-efficiencies-190416.pdf, 2019. Accessed: 28/05/2019.

[3] M. M. Lee, J. Teuscher, T. Miyasaka, T. N. Murakami, H. J. Snaith, Efficient hybrid solar cells based on meso-superstructured organometal halide perovskites, Science 338 (2012) 643–647. URL: https://science.sciencemag.org/content/338/6107/643. doi:10.1126/science.1228604. arXiv:https://science.sciencemag.org/content/338/6107/643.full.pdf.

[4] H.-S. Kim, C.-R. Lee, J.-H. Im, K.-B. Lee, T. Moehl, A. Marchioro, S.-J. Moon, R. Humphry-Baker, J.-H. Yum, J. E. Moser, et al., Lead iodide perovskite sensitized all-solid-state submicron thin film mesoscopic solar cell with efficiency exceeding 9%, Scientific reports 2 (2012) 591.

[5] D. B. Mitzi, C. Feild, W. Harrison, A. Guloy, Conducting tin halides with a layered organic-based perovskite structure, Nature 369 (1994) 467.

[6] J. E. Carlé, M. Helgesen, O. Hagemann, M. Hösel, I. M. Heckler, E. Bundgaard, S. A. Gevorgyan, R. R. Søndergaard, M. Jørgensen, R. García-Valverde, S. Chaouki-Almagro, J. A. Villarejo, F. C. Krebs, Overcoming the scaling lag for polymer solar cells, Joule 1 (2017) 274 – 289. URL: http://www.sciencedirect.com/science/article/pii/S2542435117300272. doi:https://doi.org/10.1016/j.joule.2017.08.002.

[7] P. Sommer-Larsen, M. Jørgensen, R. R. Søndergaard, M. Hösel, F. C. Krebs, It is all in the pattern—high-efficiency power extraction from polymer solar cells through high-voltage serial connection, Energy Technology 1 (2013) 15–19. URL: https://onlinelibrary.wiley.com/doi/abs/10.1002/ente.201200055. doi:10.1002/ente.201200055. arXiv:https://onlinelibrary.wiley.com/doi/pdf/10.1002/ente.201200055.

[8] N. Espinosa, M. Hösel, M. Jørgensen, F. C. Krebs, Large scale deployment of polymer solar cells on land, on sea and in the air, Energy Environ. Sci. 7 (2014) 855–866. URL: http://dx.doi.org/10.1039/C3EE43212B. doi:10.1039/C3EE43212B.

[9] Y. Deng, E. Peng, Y. Shao, Z. Xiao, Q. Dong, J. Huang, Scalable fabrication of efficient organolead trihalide perovskite solar cells with doctor-bladed active layers, Energy Environ. Sci. 8 (2015) 1544–1550. URL: http://dx.doi.org/10.1039/C4EE03907F. doi:10.1039/C4EE03907F.

[10] A. Mei, X. Li, L. Liu, Z. Ku, T. Liu, Y. Rong, M. Xu, M. Hu, J. Chen, Y. Yang, M. Grätzel, H. Han, A hole-conductor–free, fully printable mesoscopic perovskite solar cell with high stability, Science 345 (2014) 295–298. URL: https://science.sciencemag.org/content/345/6194/295. doi:10.1126/science.1254763. arXiv:https://science.sciencemag.org/content/345/6194/295.full.pdf.

[11] J. E. Bishop, T. J. Routledge, D. G. Lidzey, Advances in spray-cast perovskite solar cells, The Journal of Physical Chemistry Letters 9 (2018) 1977–1984. URL: https://doi.org/10.1021/acs.jpclett.8b00311. doi:10.1021/acs.jpclett.8b00311. arXiv:https://doi.org/10.1021/acs.jpclett.8b00311, pMID: 29608061.

[12] H. Huang, J. Shi, L. Zhu, D. Li, Y. Luo, Q. Meng, Two-step ultrasonic spray deposition of ch3nh3pbi3 for efficient and large-area perovskite solar cell, Nano Energy 27 (2016) 352 – 358. URL: http://www.sciencedirect.com/science/article/pii/S2211285516302658. doi:https://doi.org/10.1016/j.nanoen.2016.07.026.

[13] Y. Y. Kim, T.-Y. Yang, R. Suhonen, M. Välimäki, T. Maaninen, A. Kemppainen, N. J. Jeon, J. Seo, Gravure-printed flexible perovskite solar cells: Toward roll-to-roll manufacturing, Advanced Science 6 (2019) 1802094. URL: https://onlinelibrary.wiley.com/doi/abs/10.1002/advs.201802094. doi:10.1002/advs.201802094. arXiv:https://onlinelibrary.wiley.com/doi/pdf/10.1002/advs.201802094.

[14] C. Momblona, L. Gil-Escrig, E. Bandiello, E. M. Hutter, M. Sessolo, K. Lederer, J. Blochwitz-Nimoth, H. J. Bolink, Efficient vacuum deposited p-i-n and n-i-p perovskite solar cells employing doped charge transport layers, Energy Environ. Sci. 9 (2016) 3456–3463. URL: http://dx.doi.org/10.1039/C6EE02100J. doi:10.1039/C6EE02100J.

[15] Y. Deng, X. Zheng, Y. Bai, Q. Wang, J. Zhao, J. Huang, Surfactant-controlled ink drying enables high-speed deposition of perovskite films for efficient photovoltaic modules, Nature Energy 3 (2018) 560–566. URL: https://doi.org/10.1038/s41560-018-0153-9. doi:10.1038/s41560-018-0153-9.

[16] K. Hwang, Y.-S. Jung, Y.-J. Heo, F. H. Scholes, S. E. Watkins, J. Subbiah, D. J. Jones, D.-Y. Kim, D. Vak, Toward large scale roll-to-roll production of fully printed perovskite solar cells, Advanced Materials 27 (2015) 1241–1247. URL: https://onlinelibrary.wiley.com/doi/abs/10.1002/adma.201404598. doi:10.1002/adma.201404598. arXiv:https://onlinelibrary.wiley.com/doi

[17] C. Zuo, D. Vak, D. Angmo, L. Ding, M. Gao, One-step roll-to-roll air processed high efficiency perovskite solar cells, Nano Energy 46 (2018) 185 – 192. URL: http://www.sciencedirect.com/science/article/pii/S2211285518300473. doi:https://doi.org/10.1016/j.nanoen.2018.01.037.

[18] Y.-J. Heo, J.-E. Kim, H. Weerasinghe, D. Angmo, T. Qin, K. Sears, K. Hwang, Y.-S. Jung, J. Subbiah, D. J. Jones, M. Gao, D.-Y. Kim, D. Vak, Printing-friendly sequential deposition via intra-additive approach for roll-to-roll process of perovskite solar cells, Nano Energy 41 (2017) 443 – 451. URL: http://www.sciencedirect.com/science/article/pii/S2211285517305923. doi:https://doi.org/10.1016/j.nanoen.2017.09.051.

[19] Y. Galagan, F. Di Giacomo, H. Gorter, G. Kirchner, I. de Vries, R. Andriessen, P. Groen, Roll-to-roll slot die coated perovskite for efficient flexible solar cells, Advanced Energy Materials 8 (2018) 1801935. URL: https://onlinelibrary.wiley.com/doi/abs/10.1002/aenm.201801935. doi:10.1002/aenm.201801935. arXiv:https://onlinelibrary.wiley.com/doi

[20] B. Dou, J. B. Whitaker, K. Bruening, D. T. Moore, L. M. Wheeler, J. Ryter, N. J. Breslin, J. J. Berry, S. M. Garner, F. S. Barnes, S. E. Shaheen, C. J. Tassone, K. Zhu, M. F. A. M. van Hest, Roll-to-roll printing of perovskite solar cells, ACS Energy Letters 3 (2018) 2558–2565. URL: https://doi.org/10.1021/acsenergylett.8b01556. doi:10.1021/acsenergylett.8b01556. arXiv:https://doi.org/10.1021/acsener

[21] D. Burkitt, P. Greenwood, K. Hooper, D. Richards, V. Stoichkov, D. Beynon, E. Jewell, T. Watson, Meniscus guide slot-die coating for roll-to-roll perovskite solar cells, MRS Advances 4 (2019) 1399–1407. doi:10.1557/adv.2019.79.

[22] M. S. Carvalho, H. S. Kheshgi, Low-flow limit in slot coating: Theory and experiments, AIChE Journal 46 (2000) 1907–1917. URL: https://aiche.onlinelibrary.wiley.com/doi/abs/10.1002/aic.690461. doi:10.1002/aic.690461003. arXiv:https://aiche.onlinelibrary.wiley.com

[23] X. Ding, J. Liu, T. A. L. Harris, A review of the operating limits in slot die coating processes, AIChE Journal 62 (2016) 2508–2524. URL: https://aiche.onlinelibrary.wiley.com/doi/abs/10.1002/aic.15268. doi:10.1002/aic.15268. arXiv:https://aiche.onlinelibrary.wiley.com/do

[24] K. Liang, D. B. Mitzi, M. T. Prikas, Synthesis and characterization of organic-inorganic perovskite thin films prepared using a versatile two-step dipping technique, Chemistry of Materials 10 (1998) 403–411. URL: https://doi.org/10.1021/cm970568f. doi:10.1021/cm970568f. arXiv:https://doi.org/10.1021/cm970568f.

[25] J. Burschka, N. Pellet, S.-J. Moon, R. Humphry-Baker, P. Gao, M. K. Nazeeruddin, M. Grätzel, Sequential deposition as a route to high-performance perovskite-sensitized solar cells, Nature 499 (2013) 316 EP –. URL: https://doi.org/10.1038/nature12340.

[26] N. J. Jeon, J. H. Noh, Y. C. Kim, W. S. Yang, S. Ryu, S. I. Seok, Solvent engineering for high-performance inorganic-organic hybrid perovskite solar cells, Nature Materials 13 (2014) 897 EP –. URL: https://doi.org/10.1038/nmat4014, article.

[27] T. M. Schmidt, T. T. Larsen-Olsen, J. E. Carlé, D. Angmo, F. C. Krebs, Upscaling of perovskite solar cells: Fully ambient roll processing of flexible perovskite solar cells with printed back electrodes, Advanced Energy Materials 5 (2015) 1500569. URL: https://onlinelibrary.wiley.com/doi/abs/10.1002/aenm.201500569. doi:10.1002/aenm.201500569. arXiv:https://onlinelibrary.wiley.com/doi

[28] J.-H. Im, H.-S. Kim, N.-G. Park, Morphology-photovoltaic property correlation in perovskite solar cells: One-step versus two-step deposition of ch3nh3pbi3, APL Materials 2 (2014) 081510. URL: https://doi.org/10.1063/1.4891275. doi:10.1063/1.4891275. arXiv:https://doi.org/10.1063/1.4891275.

[29] J. A. Baker, Y. Mouhamad, K. E. A. Hooper, D. Burkitt, M. Geoghe-

gan, T. M. Watson, From spin coating to roll-to-roll: investigating the challenge of upscaling lead halide perovskite solar cells, IET Renewable Power Generation 11 (2017) 546–549. doi:10.1049/iet-rpg.2016.0683.

[30] T. Zhang, M. Yang, Y. Zhao, K. Zhu, Controllable sequential deposition of planar ch3nh3pbi3 perovskite films via adjustable volume expansion, Nano Letters 15 (2015) 3959–3963. URL: https://doi.org/10.1021/acs.nanolett.5b00843 doi:10.1021/acs.nanolett.5b00843. arXiv:https://doi.org/10.1021/acs.nanolett.5b00843. pMID: 25996160.

[31] Y. Xie, F. Shao, Y. Wang, T. Xu, D. Wang, F. Huang, Enhanced performance of perovskite ch3nh3pbi3 solar cell by using ch3nh3i as additive in sequential deposition, ACS Applied Materials & Interfaces 7 (2015) 12937–12942. URL: https://doi.org/10.1021/acsami.5b02705 doi:10.1021/acsami.5b02705. arXiv:https://doi.org/10.1021/acsami.5b02705. pMID: 26009927.

[32] C. Gong, S. Tong, K. Huang, H. Li, H. Huang, J. Zhang, J. Yang, Flexible planar heterojunction perovskite solar cells fabricated via sequential roll-to-roll microgravure printing and slot-die coating deposition, Solar RRL (????).

[33] Y. Y. Kim, E. Y. Park, T.-Y. Yang, J. H. Noh, T. J. Shin, N. J. Jeon, J. Seo, Fast two-step deposition of perovskite via mediator extraction treatment for large-area, high-performance perovskite solar cells, J. Mater. Chem. A 6 (2018) 12447–12454. URL: http://dx.doi.org/10.1039/C8TA02868K doi:10.1039/C8TA02868K.

[34] Y.-C. Huang, C.-F. Li, Z.-H. Huang, P.-H. Liu, C.-S. Tsao, Rapid and sheet-to-sheet slot-die coating manufacture of highly efficient perovskite solar cells processed under ambient air, Solar Energy 177 (2019) 255 – 261. URL: http://www.sciencedirect.com/science/article/pii/S0038092X18311204 doi:https://doi.org/10.1016/j.solener.2018.11.020.

[35] M. Remeika, L. K. Ono, M. Maeda, Z. Hu, Y. Qi, High-throughput surface preparation for flexible slot die coated perovskite solar cells, Organic Electronics 54 (2018) 72 – 79. URL: http://www.sciencedirect.com/science/article/pii/S1566119917306237 doi:https://doi.org/10.1016/j.orgel.2017.12.027.

[36] D. Burkitt, J. Searle, D. A. Worsley, T. Watson, Sequential slot-die deposition of perovskite solar cells using dimethylsulfoxide lead iodide ink, Materials 11 (2018). URL: http://www.mdpi.com/1996-1944/11/11/2106 doi:10.3390/ma11112106.

[37] T. A. Berhe, W.-N. Su, C.-H. Chen, C.-J. Pan, J.-H. Cheng, H.-M. Chen, M.-C. Tsai, L.-Y. Chen, A. A. Dubale, B.-J. Hwang, Organometal halide perovskite solar cells: degradation and stability, Energy Environ. Sci. 9 (2016) 323–356. URL: http://dx.doi.org/10.1039/C5EE02733K doi:10.1039/C5EE02733K.

[38] N. H. Tiep, Z. Ku, H. J. Fan, Recent advances in improving the stability of perovskite solar cells, Advanced Energy Materials 6 (2016) 1501420. URL: https://onlinelibrary.wiley.com/doi/abs/10.1002/aenm.201501420 doi:10.1002/aenm.201501420. arXiv:https://onlinelibrary.wiley.com/doi/pdf/10.1002/aenm.201501420.

[39] M. P. de Jong, L. J. van IJzendoorn, M. J. A. de Voigt, Stability of the interface between indium-tin-oxide and poly(3,4-ethylenedioxythiophene)/poly(styrenesulfonate) in polymer light-emitting diodes, Applied Physics Letters 77 (2000) 2255–2257. URL: https://doi.org/10.1063/1.1315344. doi:10.1063/1.1315344. arXiv:https://doi.org/10.1063/1.1315344.

[40] Q. Jiang, X. Zhang, J. You, Sno2: A wonderful electron transport layer for perovskite solar cells, Small 14 (2018) 1801154. URL: https://onlinelibrary.wiley.com/doi/abs/10.1002/smll.201801154 doi:10.1002/smll.201801154. arXiv:https://onlinelibrary.wiley.com/doi/pdf/10.1002/smll.201801154.

[41] G. Cotella, J. Baker, D. Worsley, F. D. Rossi, C. Pleydell-Pearce, M. Carnie, T. Watson, One-step deposition by slot-die coating of mixed lead halide perovskite for photovoltaic applications, Solar Energy Materials and Solar Cells 159 (2017) 362 – 369. URL: http://www.sciencedirect.com/science/article/pii/S0927024816303518 doi:https://doi.org/10.1016/j.solmat.2016.09.013.

[42] D. Burkitt, J. Searle, T. Watson, Perovskite solar cells in n-i-p structure with four slot-die-coated layers, Royal Society Open Science 5 (2018) 172158. URL: https://royalsocietypublishing.org/doi/abs/10.1098/rsos.172158 doi:10.1098/rsos.172158. arXiv:https://royalsocietypublishing.org/doi/

[43] J.-E. Kim, Y.-S. Jung, Y.-J. Heo, K. Hwang, T. Qin, D.-Y. Kim, D. Vak, Slot die coated planar perovskite solar cells via blowing and heating assisted one step deposition, Solar Energy Materials and Solar Cells 179 (2018) 80 – 86. URL: http://www.sciencedirect.com/science/article/pii/S0927024818300543 doi:https://doi.org/10.1016/j.solmat.2018.02.003.

[44] J. C. Cruz, J. Mejía-Escobar, F. Jaramillo, Slot-die processing of flexible perovskite solar cells in ambient conditions, Solar Energy 150 (2017) 570 – 576. URL: http://www.sciencedirect.com/science/article/pii/S0038092X17303705 doi:https://doi.org/10.1016/j.solener.2017.04.071.

[45] D. Lee, Y.-S. Jung, Y.-J. Heo, S. Lee, K. Hwang, Y.-J. Jeon, J.-E. Kim, J. Park, G. Y. Jung, D.-Y. Kim, Slot-die coated perovskite films using mixed lead precursors for highly reproducible and large-area solar cells, ACS Applied Materials & Interfaces 10 (2018) 16133–16139. URL: https://doi.org/10.1021/acsami.8b02549 doi:10.1021/acsami.8b02549. arXiv:https://doi.org/10.1021/acsami.8b02549. pMID: 29668247.

[46] W. Zhang, M. Saliba, D. T. Moore, S. K. Pathak, M. T. Hörantner, T. Stergiopoulos, S. D. Stranks, G. E. Eperon, J. A. Alexander-Webber, A. Abate, A. Sadhanala, S. Yao, Y. Chen, R. H. Friend, L. A. Estroff, U. Wiesner, H. J. Snaith, Ultrasmooth organic-inorganic perovskite thin-film formation and crystallization for efficient planar heterojunction solar cells, Nature Communications 6 (2015) 6142 EP –. URL: https://doi.org/10.1038/ncomms7142, article.

[47] C. Kamaraki, A. Zachariadis, C. Kapnopoulos, E. Mekeridis, C. Gravalidis, A. Laskarakis, S. Logothetidis, Efficient flexible printed perovskite solar cells based on lead acetate precursor, Solar Energy 176 (2018) 406 – 411. URL: http://www.sciencedirect.com/science/article/pii/S0038092X18310304 doi:https://doi.org/10.1016/j.solener.2018.10.055.

[48] F. D. Giacomo, S. Shanmugam, H. Fledderus, B. J. Bruijnaers, W. J. Verhees, M. S. Dorenkamper, S. C. Veenstra, W. Qiu, R. Gehlhaar, T. Merckx, T. Aernouts, R. Andriessen, Y. Galagan, Up-scalable sheet-to-sheet production of high efficiency perovskite module and solar cells on 6-in. substrate using slot die coating, Solar Energy Materials and Solar Cells 181 (2018) 53 – 59. URL: http://www.sciencedirect.com/science/article/pii/S0927024817306127 doi:https://doi.org/10.1016/j.solmat.2017.11.010, thin film solar cells and applications.

[49] Y.-S. Jung, K. Hwang, Y.-J. Heo, J.-E. Kim, D. Lee, C.-H. Lee, H.-I. Joh, J.-S. Yeo, D.-Y. Kim, One-step printable perovskite films fabricated under ambient conditions for efficient and reproducible solar cells, ACS Applied Materials & Interfaces 9 (2017) 27832–27838. URL: https://doi.org/10.1021/acsami.7b05078 doi:10.1021/acsami.7b05078. arXiv:https://doi.org/10.1021/acsami.7b05078. pMID: 28752996.

[50] S. Bae, S. J. Han, T. J. Shin, W. H. Jo, Two different mechanisms of ch3nh3pbi3 film formation in one-step deposition and photovoltaic properties of opv-type perovskite solar cells, J. Mater. Chem. A 3 (2015) 23964–23972. URL: http://dx.doi.org/10.1039/C5TA06870C doi:10.1039/C5TA06870C.

[51] J. B. Whitaker, D. H. Kim, B. W. Larson, F. Zhang, J. J. Berry, M. F. A. M. van Hest, K. Zhu, Scalable slot-die coating of high performance perovskite solar cells, Sustainable Energy Fuels 2 (2018) 2442–2449. URL: http://dx.doi.org/10.1039/C8SE00368H doi:10.1039/C8SE00368H.

[52] N. K. Noel, S. N. Habisreutinger, B. Wenger, M. T. Klug, M. T. Hörantner, M. B. Johnston, R. J. Nicholas, D. T. Moore, H. J. Snaith, A low viscosity, low boiling point, clean solvent system for the rapid crystallisation of highly specular perovskite films, Energy Environ. Sci. 10 (2017) 145–152. URL: http://dx.doi.org/10.1039/C6EE02373H doi:10.1039/C6EE02373H.

[53] H. Li, Y. Pan, Z. Wang, Y. Xia, Y. Chen, W. Huang, Additive engineering for highly efficient organic–inorganic halide perovskite solar cells: recent advances and perspectives, J. Mater. Chem. A 5 (2017) 12602–12652. URL: http://dx.doi.org/10.1039/C7TA01798G doi:10.1039/C7TA01798G.

[54] Z. Gu, L. Zuo, T. T. Larsen-Olsen, T. Ye, G. Wu, F. C. Krebs,

H. Chen, Interfacial engineering of self-assembled monolayer modified semi-roll-to-roll planar heterojunction perovskite solar cells on flexible substrates, J. Mater. Chem. A 3 (2015) 24254–24260. URL: http://dx.doi.org/10.1039/C5TA07008B. doi:10.1039/C5TA07008B.

[55] J.-E. Kim, S.-S. Kim, C. Zuo, M. Gao, D. Vak, D.-Y. Kim, Humidity-tolerant roll-to-roll fabrication of perovskite solar cells via polymer-additive-assisted hot slot die deposition, Advanced Functional Materials 0 (????) 1809194. URL: https://onlinelibrary.wiley.com/doi/abs/10.1002/adfm.201809194. doi:10.1002/adfm.201809194. arXiv:https://onlinelibrary.wiley.com/doi/pdf/10.1002/adfm.201809194.

[56] J. Yan, W. Qiu, G. Wu, P. Heremans, H. Chen, Recent progress in 2d/quasi-2d layered metal halide perovskites for solar cells, J. Mater. Chem. A 6 (2018) 11063–11077. URL: http://dx.doi.org/10.1039/C8TA02288G. doi:10.1039/C8TA02288G.

[57] W. Fu, J. Wang, L. Zuo, K. Gao, F. Liu, D. S. Ginger, A. K.-Y. Jen, Two-dimensional perovskite solar cells with 14.1% power conversion efficiency and 0.68% external radiative efficiency, ACS Energy Letters 3 (2018) 2086–2093. URL: https://doi.org/10.1021/acsenergylett.8b01181. doi:10.1021/acsenergylett.8b01181. arXiv:https://doi.org/10.1021/acsenergylett.8b01181.

[58] C. Zuo, A. D. Scully, D. Vak, W. Tan, X. Jiao, C. R. McNeill, D. Angmo, L. Ding, M. Gao, Self-assembled 2d perovskite layers for efficient printable solar cells, Advanced Energy Materials 9 (2019) 1803258. URL: https://onlinelibrary.wiley.com/doi/abs/10.1002/aenm.201803258. doi:10.1002/aenm.201803258. arXiv:https://onlinelibrary.wiley.com/doi/pdf/10.1002/aenm.201803258.

[59] G. Murugadoss, H. Kanda, S. Tanaka, H. Nishino, S. Ito, H. Imahori, T. Umeyama, An efficient electron transport material of tin oxide for planar structure perovskite solar cells, Journal of Power Sources 307 (2016) 891 – 897. URL: http://www.sciencedirect.com/science/article/pii/S0378775316320441. doi:https://doi.org/10.1016/j.jpowsour.2016.01.044.

[60] T. Supasai, N. Henjongchom, I.-M. Tang, F. Deng, N. Rujisamphan, Compact nanostructured tio2 deposited by aerosol spray pyrolysis for the hole-blocking layer in a ch3nh3pbi3 perovskite solar cell, Solar Energy 136 (2016) 515 – 524. URL: http://www.sciencedirect.com/science/article/pii/S0038092X16302936. doi:https://doi.org/10.1016/j.solener.2016.07.035.

[61] T. Bu, J. Li, F. Zheng, W. Chen, X. Wen, Z. Ku, Y. Peng, J. Zhong, Y.-B. Cheng, F. Huang, Universal passivation strategy to slot-die printed sno2 for hysteresis-free efficient flexible perovskite solar module, Nature Communications 9 (2018) 4609. URL: https://doi.org/10.1038/s41467-018-07099-9. doi:10.1038/s41467-018-07099-9.

[62] R. R. Søndergaard, M. Hösel, F. C. Krebs, Roll-to-roll fabrication of large area functional organic materials, Journal of Polymer Science Part B: Polymer Physics 51 (2013) 16–34. URL: https://onlinelibrary.wiley.com/doi/abs/10.1002/polb.23192. doi:10.1002/polb.23192. arXiv:https://onlinelibrary.wiley.com/doi/pdf/10.1002/polb.23192.

[63] P. Zhang, J. Wu, T. Zhang, Y. Wang, D. Liu, H. Chen, L. Ji, C. Liu, W. Ahmad, Z. D. Chen, S. Li, Perovskite solar cells with zno electron-transporting materials, Advanced Materials 30 (2018) 1703737. URL: https://onlinelibrary.wiley.com/doi/abs/10.1002/adma.201703737. doi:10.1002/adma.201703737. arXiv:https://onlinelibrary.wiley.com/doi/pdf/10.1002/adma.201703737.

[64] I. M. Hossain, D. Hudry, F. Mathies, T. Abzieher, S. Moghadamzadeh, D. Rueda-Delgado, F. Schackmar, M. Bruns, R. Andriessen, T. Aernouts, F. Di Giacomo, U. Lemmer, B. S. Richards, U. W. Paetzold, A. Hadipour, Scalable processing of low-temperature tio2 nanoparticles for high-efficiency perovskite solar cells, ACS Applied Energy Materials 2 (2019) 47–58. URL: https://doi.org/10.1021/acsaem.8b01567. doi:10.1021/acsaem.8b01567. arXiv:https://doi.org/10.1021/acsaem.8b01567.

[65] C. Zuo, L. Ding, Modified pedot layer makes a 1.52 v voc for perovskite/pcbm solar cells, Advanced Energy Materials 7 (2017) 1601193. URL: https://onlinelibrary.wiley.com/doi/abs/10.1002/aenm.201601193. doi:10.1002/aenm.201601193. arXiv:https://onlinelibrary.wiley.com/doi/pdf/10.1002/aenm.201601193.

[66] J.-S. Yeo, C.-H. Lee, D. Jang, S. Lee, S. M. Jo, H.-I. Joh, D.-Y. Kim, Reduced graphene oxide-assisted crystallization of perovskite via solution-process for efficient and stable planar solar cells with module-scales, Nano Energy 30 (2016) 667 – 676. URL: http://www.sciencedirect.com/science/article/pii/S2211285516304811. doi:https://doi.org/10.1016/j.nanoen.2016.10.065.

[67] F. D. Giacomo, H. Fledderus, H. Gorter, G. Kirchner, I. d. Vries, I. Dogan, W. Verhees, V. Zardetto, M. Najafi, D. Zhang, H. Lifka, Y. Galagan, T. Aernouts, S. Veenstra, P. Groen, R. Andriesse, Large area ¿140cm2 perovskite solar modules made by sheet to sheet and roll to roll fabrication with 14.5% efficiency (2018) 2795–2798. doi:10.1109/PVSC.2018.8548157.

[68] K. K. Sears, M. Fievez, M. Gao, H. C. Weerasinghe, C. D. Easton, D. Vak, Ito-free flexible perovskite solar cells based on roll-to-roll, slot-die processing, Solar RRL 1 (2017) 1700059. URL: https://onlinelibrary.wiley.com/doi/abs/10.1002/solr.201700059. doi:10.1002/solr.201700059. arXiv:https://onlinelibrary.wiley.com/doi/

[69] F. Guo, H. Azimi, Y. Hou, T. Przybilla, M. Hu, C. Bronnbauer, S. Langner, E. Spiecker, K. Forberich, C. J. Brabec, High-performance semitransparent perovskite solar cells with solution-processed silver nanowires as top electrodes, Nanoscale 7 (2015) 1642–1649. URL: http://dx.doi.org/10.1039/C4NR06033D. doi:10.1039/C4NR06033D.

[70] M. Xie, H. Lu, L. Zhang, J. Wang, Q. Luo, J. Lin, L. Ba, H. Liu, W. Shen, L. Shi, C.-Q. Ma, Fully solution-processed semitransparent perovskite solar cells with ink-jet printed silver nanowires top electrode, Solar RRL 2 (2018) 1700184. URL: https://onlinelibrary.wiley.com/doi/abs/10.1002/solr.201700184. doi:10.1002/solr.201700184. arXiv:https://onlinelibrary.wiley.com/doi/

[71] S. Tong, C. Gong, C. Zhang, G. Liu, D. Zhang, C. Zhou, S. Shi, X. Gao, J. Yang, Fully-printed, flexible cesium-doped triple cation perovskite photodetector, Applied Materials Today 15 (2019) 389 – 397. URL: http://www.sciencedirect.com/science/article/pii/S2352940718307676. doi:https://doi.org/10.1016/j.apmt.2019.03.001.

[72] M. Prakasam, D. Tordera, F. Di Giacomo, R. Abbel, A. Langen, G. Gelinck, H. J. Bolink, Large area perovskite light-emitting diodes by gas-assisted crystallization, J. Mater. Chem. C 7 (2019) 3795–3801. URL: http://dx.doi.org/10.1039/C8TC06482B. doi:10.1039/C8TC06482B.